AGU PUBLICATIONS

JGR

Journal of Geophysical Research: Space Physics

RESEARCH ARTICLE
10.1002/2015JA021089

Special Section:
Low-Frequency Waves in Space Plasmas

Statistical characteristics of EMIC waves: Van Allen Probe observations

Dedong Wang[1], Zhigang Yuan[1], Xiongdong Yu[1], Xiaohua Deng[1,2], Meng Zhou[2], Shiyong Huang[1], Haimeng Li[1], Zhenzhen Wang[1], Zheng Qiao[1], C. A. Kletzing[3], and J. R. Wygant[4]

[1]School of Electronic Information, Wuhan University, Wuhan, China, [2]Institute of Space Science and Technology, Nanchang University, Nanchang, China, [3]Department of Physics and Astronomy, University of Iowa, Iowa City, Iowa, USA, [4]School of Physics and Astronomy, University of Minnesota, Minneapolis, Minnesota, USA

Key Points:
- The distribution character of EMIC waves in lower *L* Shells is studied
- EMIC waves distribute relatively uniform in the MLT sectors in lower *L* shells
- EMIC waves in the dawn sector at low *L* shell are significant

Correspondence to:
Z. Yuan,
y_zgang@vip.163.com

Citation:
Wang, D., et al. (2015), Statistical characteristics of EMIC waves: Van Allen Probe observations, *J. Geophys. Res. Space Physics, 120*, 4400–4408, doi:10.1002/2015JA021089.

Received 5 FEB 2015
Accepted 4 MAY 2015
Accepted article online 8 MAY 2015
Published online 4 JUN 2015
Corrected 22 JAN 2016

This article was corrected on 22 JAN 2016. See the end of the full text for details.

Abstract Utilizing the data from the magnetometer instrument which is a part of the Electric and Magnetic Field Instrument Suite and Integrated Science instrument suite on board the Van Allen Probe A from September 2012 to April 2014, when the apogee of the satellite has passed all the magnetic local time (MLT) sectors, we obtain the statistical distribution characteristics of electromagnetic ion cyclotron (EMIC) waves in the inner magnetosphere over all magnetic local times from $L = 3$ to $L = 6$. Compared with the previous statistical results about EMIC waves, the occurrence rates of EMIC waves distribute relatively uniform in the MLT sectors in lower *L* shells. On the other hand, in higher *L* shells, there are indeed some peaks of the occurrence rate for the EMIC waves, especially in the noon, dusk, and night sectors. EMIC waves appear at lower *L* shells in the dawn sector than in other sectors. In the lower *L* shells ($L < 4$), the occurrence rates of EMIC waves are significant in the dawn sector. This phenomenon may result from the distribution characteristics of the plasmasphere. The location of the plasmapause is usually lower in the dawn sector than that in other sectors, and the plasmapause is considered to be the favored region for the generation of EMIC waves. In higher *L* shells ($L > 4$) the occurrence rates of EMIC waves are most significant in the dusk sector, implying the important role of the plasmapause or plasmaspheric plume in generating EMIC waves. We have also investigated the distribution characteristics of the hydrogen band and the helium band EMIC waves. Surprisingly, in the inner magnetosphere, the hydrogen band EMIC waves occur more frequently than the helium band EMIC waves. Both of them have peaks of occurrence rate in noon, dusk, and night sectors, and the hydrogen band EMIC waves have more obvious peaks than the helium band EMIC waves in the night sector, while the helium band EMIC waves are more concentrated than the hydrogen band EMIC waves in the dusk sector. Both of them occur significantly in the noon sector, which implies the important role of the solar wind dynamic pressure.

1. Introduction

Electromagnetic ion cyclotron (EMIC) waves are discrete electromagnetic emissions, which are usually considered to be generated by the ring current ions with temperature anisotropy ($T_\perp > T_\parallel$) [*Cornwall*, 1965; *Summers and Thorne*, 2003; *Zhang et al.*, 2014]. The frequencies of EMIC waves are confined below the gyrofrequency of proton in their source region, which is considered to be near the geomagnetic equator, with (magnetic latitude) $|\mathrm{MLAT}| < 11°$ [*Loto'aniu et al.*, 2005; *Thorne*, 2010]. Due to interactions with the ion component of the background plasma, EMIC waves are divided into three bands: hydrogen band, helium band, and oxygen band. The frequency of hydrogen band EMIC waves lies between the gyrofrequency of hydrogen and helium ion at the source region, while helium band EMIC waves between helium and oxygen gyrofrequencies, and the oxygen band EMIC waves, have frequency below the gyrofrequency of oxygen at their source region. Hydrogen band EMIC waves mainly occur outside the plasmapause, while the helium band EMIC waves can be found both inside and outside the plasmapause [*Fraser and Nguyen*, 2001]. Due to their low frequency and the orbits of the former satellites, oxygen band EMIC waves are rarely reported. Taking advantage of the low orbits of the Van Allen Probes in the inner magnetosphere, some oxygen band EMIC waves are observed, which are discussed in another paper [*Yu et al.*, 2015]. EMIC waves are believed to play an important role in the dynamic evolution of the inner magnetosphere. Through wave particle interaction, they can lead to precipitations of ring current ions [*Cornwall et al.*, 1970; *Jordanova et al.*, 2001; *Keika et al.*, 2006; *Yuan et al.*, 2010, 2012; *Zhu et al.*, 2012; *Su et al.*, 2014] and relativistic electrons [*Bortnik et al.*, 2006; *Summers et al.*, 2007; *Jordanova et al.*, 2008b; *Shprits et al.*, 2009; *Su et al.*, 2010, 2011, 2012, 2013;

Yuan et al., 2013; *Hyun et al.*, 2014; *D. D. Wang et al.*, 2014]. Through Landau damping, they can also heat cold electrons in the magnetosphere [*Zhou et al.*, 2013] and plasmaspheric plume [*Yuan et al.*, 2014]. Therefore, it is necessary to investigate the distribution characteristics of EMIC waves in the inner magnetosphere, especially the distribution function about L and magnetic local time (MLT).

The cold, dense plasmas also play an important role in the generation of EMIC waves, because they can bring down the instability threshold to generate EMIC waves [*Gary et al.*, 1995]. Some theoretical and observational studies hold the view that EMIC waves are easier to be generated when the hot anisotropic ions encounter the dense and cold plasmasphere [*Gary et al.*, 1995; *Yuan et al.*, 2010; *Liu et al.*, 2013]. Plasmaspheric plumes are also suggested to be a preferential structure where EMIC waves can be generated easily [*Yuan et al.*, 2014]. On the other hand, some studies emphasize the pivotal role of the solar wind dynamic pressure in the generation of the EMIC waves [*Usanova et al.*, 2008, 2010; *McCollough et al.*, 2009, 2012]. Active Magnetospheric Particle Tracer Explorers (AMPTE) CCE observations show that EMIC waves mainly occur between 11:00 and 18:00 MLT [*Anderson et al.*, 1992a, 1992b]. Inferred from the events of simultaneous precipitation of relativistic electrons and ring current ions observed by the NOAA POES satellites, EMIC waves are found to be generally located at the dusk to midnight sectors [*Z. Wang et al.*, 2014]. Although some statistical studies claim that the occurrence rate of the EMIC waves in the inner magnetosphere is limited, just several percent [*Min et al.*, 2012; *Usanova et al.*, 2012; *Meredith et al.*, 2014], one shortcoming of the previous statistical studies is that the spacecraft such as Time History of Events and Macroscale Interactions during Substorms (THEMIS) and CRRES spent limited time in the inner magnetosphere, especially in lower L shells. The apogee of the CRRES satellite nearly reached $L = 8$, higher than that of the Van Allen Probes, and it did not covered all the MLT regions. Therefore, the occurrence rate of the EMIC waves in the inner magnetosphere need to be further assessed.

Van Allen Probes spend all their time below the geosynchronous orbit, which provides an unprecedented opportunity to study the statistical distribution characteristic of the EMIC waves in the inner magnetosphere. In this paper, utilizing the data from the Electric and Magnetic Field Instrument Suite and Integrated Science (EMFISIS) magnetometer instrument on board the Van Allen Probe A and an automated wave detection algorithm [*Bortnik et al.*, 2007], we investigate the occurrence rate of the EMIC waves in the inner magnetosphere and the characteristics of EMIC waves on the different bands.

The remained parts of this paper are organized as follows: first, an introduction about the Van Allen Probes and their onboard instruments is given; then, the algorithm of data processing is introduced, and an example of EMIC waves found by the algorithm is presented; in the fourth part of this paper, the statistical results are shown; and finally, some discussions and conclusions end this paper.

2. Van Allen Probes' Orbits and Instrumentation

The Van Allen Probes, first named Radiation Belt Storm Probes (RBSP), were launched on 30 August 2012. The identical twin spacecraft (A and B) carry on the same state-of-the-art instruments. The orbits of the Van Allen Probes are all confined below the geosynchronous orbit and lie nearly in the Earth's equatorial plane, covering the L shell range from nearly 1.1 to 6.5, which provides an unprecedented opportunity for the research in the inner magnetosphere. In this paper, we utilize the data of the Electric and Magnetic Field Instrument Suite and Integrated Science (EMFISIS) magnetometer instrument on board the Van Allen Probe A to investigate the distribution characteristics of EMIC waves. EMFISIS magnetometer instrument provides vector magnetic field measurement which measures the background magnetic field and the low-frequency waves [*Kletzing et al.*, 2013]. The sampling cadence of EMFISIS magnetometer is 64 Hz. Figure 1 illustrates the dwell time of the Van Allen Probe A during 8 September 2012 to 30 April 2014, when the apogee of this satellite covered all MLT sectors due to precession, and we choose this period to study the distribution characteristics of the EMIC waves. In Figure 1, MLT has 1 h resolution and L has 0.5 L resolution, and the unit of the color bar is hour. In addition, we choose the region from $L = 3$ to $L = 6$ and will give reasons below. To avoid the ambiguity if the twin satellites observe the same event or not, we have not utilized the data from Van Allen Probe B. On the other hand, one satellite is enough for the statistical work since its apogee has already covered all the MLT regions. At last, the data from the magnetometer instrument on board Van Allen Probe B are not so good for the automated wave detection algorithm which we utilized, because the data from the magnetometer instrument on board Van Allen Probe B contain much more noise than that from Van Allen Probe A.

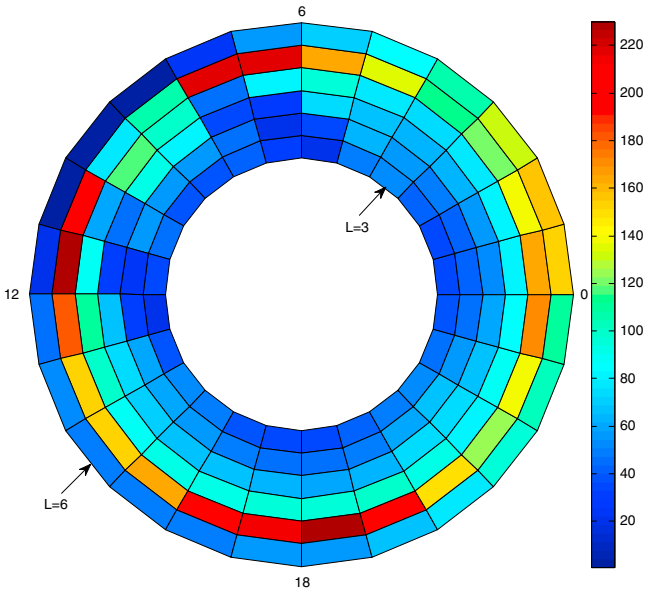

Figure 1. Dwell time distribution of the Van Allen Probe A from 8 September 2012 to 30 April 2014. The *L* shell ranges from $L = 3$ to $L = 6$. The unit for the color bar is hour.

Besides the data from EMFISIS magnetometer instrument, we also utilized the plasma density data provided from the Electric Field and Wave (EFW) instruments on board the Van Allen Probe A to check the relationship between the EMIC occurrence region and the location of the plasmapause.

3. Algorithm

First, we calculate the moving average of the original magnetic field data from the magnetometer of EMFISIS suite and subtract them from the original data to get the fluctuating magnetic field data. Applying the short time fast Fourier transform to the fluctuating magnetic field, we obtained the dynamic spectrogram, as an example shown in Figure 2. The magnetic data are sampled at 64 Hz and are processed in blocks of 1 h. The time series are divided into consecutive and overlapping time segments; each time segment is windowed by a Hamming window to reduce edge effects. In our research, the sliding window is chosen to be 6400 points (100 s) long, with an overlap of 4500 points, providing a frequency resolution of 0.01 Hz and a time resolution of about 30 s (1900/64 s). Therefore, each column of the spectrogram represents the spectral content of a time interval about 30 s.

Further, the *L* shell values covered by the Van Allen Probe are not so high (less than 7), and the oxygen gyrofrequency at geomagnetic equator with $L = 6$ is about 0.14 Hz in a dipole magnetic field model; therefore, we set the lowest frequency of interest to be 0.1 Hz, to contain the frequency range of helium band EMIC waves. Additionally, although the gyrofrequency of hydrogen at the lowest *L* can approach several tens of hertz, and the Nyquist frequency of EMFISIS magnetometer is 32 Hz, we choose 10 Hz as

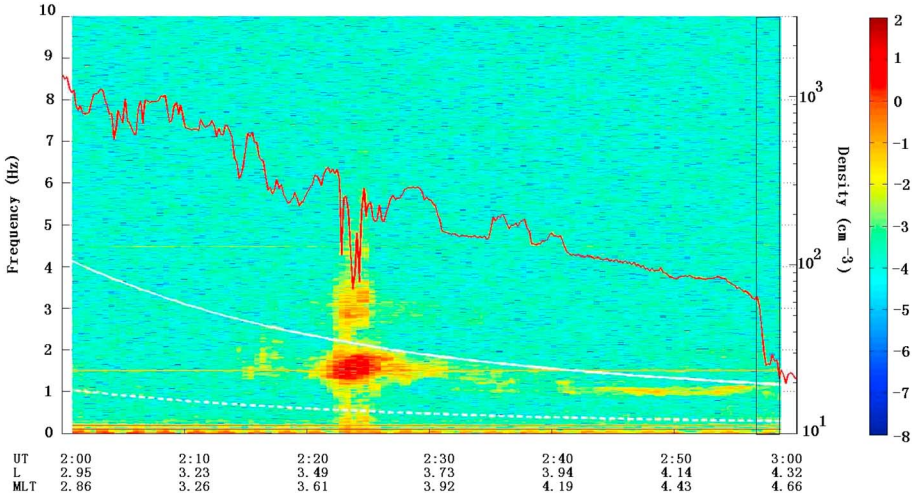

Figure 2. An example of EMIC wave events found by the algorithm. The Van Allen Probe A satellite observed these pulsations during 2:00 to 3:00 UT on 12 October 2012. The white solid line superposed on this figure illustrates the local gyrofrequency of helium, and the white dashed line shows the local gyrofrequency of oxygen. The red solid line indicates the density of the plasma. The scale of the plasma density is in the right side vertical axis of this figure. The black rectangle near 3:00 UT demonstrates the outer edge of the plasmapause.

the upper limit frequency for simplification, and we choose the region from $L = 3$ to $L = 6$ to survey. The sampling points where the gyrofrequency of hydrogen exceeds 10 Hz and below 32 Hz account for a small percentage of the total sampling points, only 15.4%, most of which locate in regions with $L < 3$. In fact, only several (~10) electromagnetic emissions, whose frequencies are higher than 10 Hz but lower than local hydrogen frequency, are found in our survey and need to be further checked. Therefore, the statistical results here can present the general characteristics of EMIC waves in the inner magnetosphere without loss of generality.

Then, an automated wave detection algorithm [*Bortnik et al*., 2007] was performed on each 1 h data blocks, as an example shown in Figure 2. At first, we performed a 3 min average to the pulsation power content. For each block which lasts 1 h, we calculated a mean background noise level. Therefore, the noise level varies from 1 h to the next. An efficient spectral point will be picked out when the 3 min average power exceeds the ambient noise level more than 1 order of magnitude in the corresponding data block, which is the same as that in *Usanova et al*. [2012]. These efficient points are divided into different data groups when the temporal separation between two efficient points is longer than a critical value [*Bortnik et al*., 2007], which is set to be 5 min in our case. Meanwhile, efficient point groups lasting less than 5 min are removed. Additionally, in some cases there are noises with constant frequency in the spectrograms, which may result from the instrument itself. In order to eliminate the effect of these noises, we set the bandwidth of the selected events to be higher than 0.1 Hz. The efficient point groups detected through the algorithm described above are identified as EMIC wave events, and the time intervals and the positions of the satellite are recorded at the same time.

Finally, the events found were verified manually to ensure the statistical results. A number of false identifications by the automated wave detection algorithm were discovered, many of which lie in the oxygen band, due to confusion with lower-frequency pulsations which are not EMIC waves, and they were removed from the event list. We indeed find some good events of oxygen band EMIC waves, but the number of which is few, so they are not included in this statistical work but in another paper [*Yu et al*., 2015].

An example of events found by the algorithm is shown in Figure 2. The white solid and dashed lines superposed on the spectrum indicate the local gyrofrequency of helium and oxygen ions, respectively. The red line in this figure depicts the density of cold plasma, the data of which are obtained from the RBSP website. On 12 October 2012, during 2:00 to 3:00 UT, some EMIC pulsations were found in the dawn sector. In our research, we treat a multiband event; i.e., EMIC waves occur on different frequency bands but in the same time interval, such as the example shown in Figure 2 during the interval from 2:15 to 2:30 UT, as a single event, as treated in *Usanova et al*. [2012]. According to our detecting algorithm, two EMIC wave events are identified in Figure 2: one appeared during 2:15–2:30 UT, while the other appeared during 2:40–2:59 UT. Both lasted more than 5 min, and the former occurred more than 5 min earlier than the latter, which are the criteria to select the wave events by the algorithm. Following the method of *Moldin et al*. [2002], we identify a plasma region with a density gradient greater than a factor of 5 within 0.5 L as the outer edge of the plasmapause. As shown in Figure 2, the black rectangle demonstrates the outer edge of the plasmapause. Therefore, both the EMIC events shown in Figure 2 occurred inside the plasmasphere.

4. Statistical Results

Applying the algorithm described above, 251 EMIC wave events have been obtained, and all of them last at least 5 min. In these events, oxygen band EMIC waves are not included, which are reported in another paper [*Yu et al*., 2015]. Figure 3a shows the distribution characteristic of the EMIC wave events found by the algorithm over all MLT and from $L = 3$ to $L = 6$; the unit of the color bar is the time interval of one spectrogram column, which represents 1900/64 s (~30 s). There are three obvious peaks on the occurrence of EMIC wave events. One peak locates at the dusk sector near the $L = 5$, which is consistent with the AMPTE/CCE observation in the sector distribution [*Anderson et al*., 1992a]. In their research, the peak concentration of events also occurs near apogee in the afternoon sector, but the apogee of AMPTE/CCE is located near $L = 9$. In Figure 3a, a strong peak occurs near the midnight sector with L from 5 to 6, which was not found obviously in AMPTE/CCE and THEMIS observations [*Anderson et al*., 1992a; *Min et al*., 2012; *Keika et al*., 2013], due to their much higher-altitude orbits. CRRES satellite, which has a similar orbit with

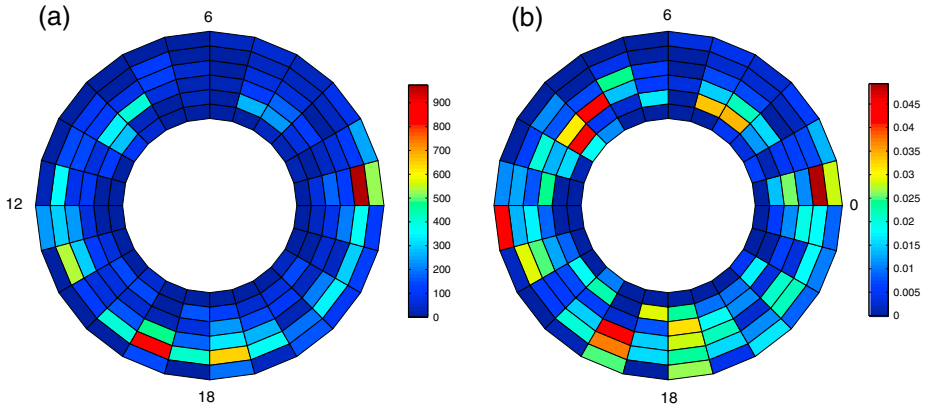

Figure 3. (a) Distribution of the EMIC wave events found by the algorithm in all MLT and from $L = 3$ to $L = 6$. The unit of the color bar is the time interval of one spectrogram column, which represents 1900/64 s (~30 s). (b) The occurrence rates of EMIC waves in all MLT and from $L = 3$ to $L = 6$.

Van Allen Probes but a higher apogee, also observed some EMIC wave events in the midnight sector with L from 5 to 6, but the peak of occurrence rate there was not so strong relatively [*Meredith et al.*, 2003, 2014]. Additionally, it is shown in Figure 3a that there is also a peak of events in the noon sector and in high L shells. The distribution characteristic of the events in the dawn sector (3:00–9:00 MLT) is consistent with that from the AMPTE/CCE observations to some extent, in which the $L > 6$ and $L < 6$ event populations appear to be radially separated in the morning, and in our research, the occurrence rate of EMIC waves indeed decreased sharply between $L = 5$ and $L = 6$ in the morning sector.

Dividing the total occurrence time interval of EMIC wave events obtained by the algorithm in each bin by the total time interval when the Van Allen Probe A was located in the corresponding bin, we obtained the occurrence rates of EMIC waves, which is shown in Figure 3b. It can be seen that the maximum occurrence rate of EMIC waves in the inner magnetosphere is indeed less than 5%, which is consistent with the previous researches [*Anderson et al.*, 1992a; *Min et al.*, 2012; *Usanova et al.*, 2012].

There are several peaks of the occurrence rates in each sector, noon (9:00–15:00 MLT), dusk (15:00–21:00 MLT), night (21:00–3:00 MLT), and the dawn (3:00–9:00 MLT) sector, which is also consistent with the AMPTE/CCE observation [*Anderson et al.*, 1992a]. In their research, the most preferred region for the EMIC waves to occur is beyond $L = 7$, while in the inner magnetosphere with $L < 5$, EMIC waves occur with a relatively uniform local time distribution. The peaks in the noon sector, dusk, and night sectors appear in higher L shell while the peaks in the dawn sector locate at lower L shell. In order to investigate the relationship between the occurrence rates and L shell in different sectors, we add the occurrence rates in the same L shell bin and in the same MLT sector together and then obtain the occurrence rates against L in different sectors. The results are shown in Figure 4, the vertical label of which indicates the occurrence rates of EMIC waves, and the horizontal label depicts the L shell region. In general, the occurrence rates between $L = 3$ and $L = 4.5$ enhance with increasing L shell values, while the occurrence rates between $L = 4.5$ and $L = 6$ decrease with increasing L shell values. Maybe the reason lies on the position of plasmapause, which is considered to be the preferred region for the excitation of EMIC waves [*Gary et al.*, 1995;

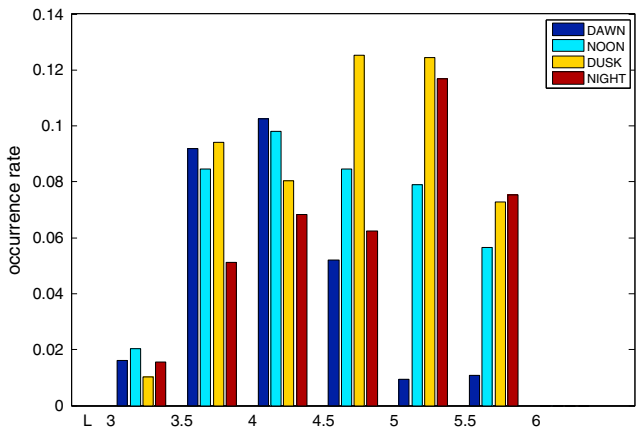

Figure 4. Diagram illustrates the occurrence rate of EMIC waves in different sectors and different L shells.

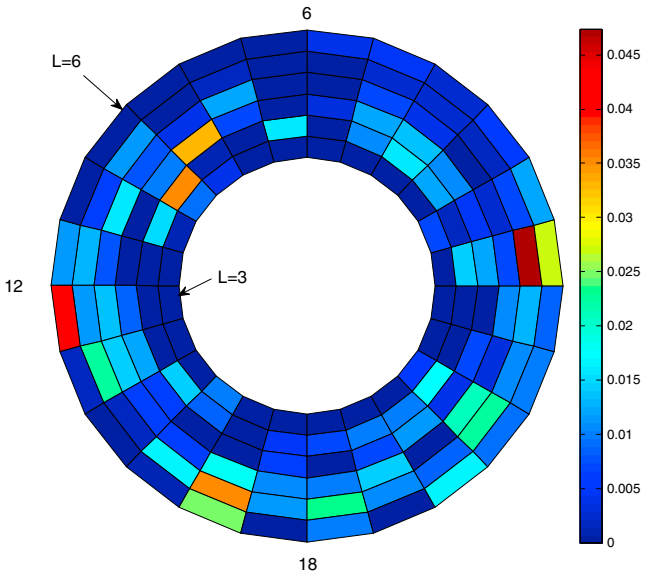

Figure 5. The occurrence rate of hydrogen band EMIC waves in all MLT and from $L = 3$ to $L = 6$.

Yuan et al., 2010] and is reported to be usually located near $L = 4$~5 [*Sheeley et al.*, 2001]. Especially at the $L = 3.5$~4, the occurrence rates in all the four sectors rise sharply, compared to those in lower region, and interestingly, the occurrence rate in the dawn sector which is believed to be low in many studies [*Keika et al.*, 2013; *Meredith et al.*, 2014] is high, comparable with those in other sectors. The occurrence rates of EMIC waves in the dawn and noon sectors grow to their own peaks at the $L = 4$~4.5 and then decrease with L, while the occurrence rate of EMIC waves in the dusk sector increases to the highest at the $L = 4.5$~5.5. At the $L = 5$~5.5, the occurrence rate in the night sector grows to its own peak.

The occurrence rates on the different band EMIC waves are also studied. As the orbits of Van Allen Probes are near the geomagnetic equator, which coincide with the generation region of EMIC waves, we utilize the local gyrofrequencies of hydrogen, helium, and oxygen ion to identify the band of EMIC waves. Previous studies utilizing satellites near the equator such as GOES [*Fraser et al.*, 2010] also treat this way. The same method has been taken in some event analyses utilizing Van Allen Probes [*Usanova et al.*, 2014]. We have also rechecked the events with $|\mathrm{MLAT}| > 11°$ with the equatorial gyrofrequencies, in order to make sure the category of hydrogen and helium band EMIC waves. In our research, 178 hydrogen band EMIC wave events were found. Figure 5 illustrates the occurrence rate distribution of hydrogen band EMIC waves, in the same format as that in Figure 3. Hydrogen band EMIC waves also have peaks of occurrence rates in every sector. Two significant peaks occur in the midnoon and midnight sectors. Peaks in the dawn sector are located at lower L shells. There are also some peaks of occurrence rates in the dusk sector at higher L shells.

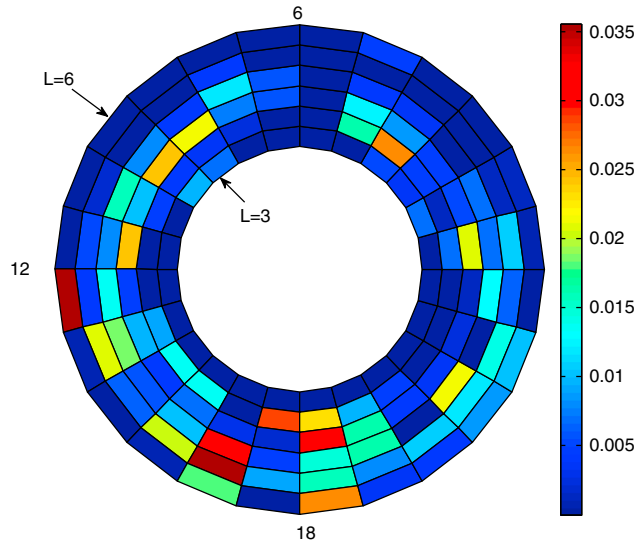

Figure 6. The occurrence rate of helium band EMIC waves in all MLT and from $L = 3$ to $L = 6$.

Additionally, for helium band EMIC waves, 154 events were found, less than that of the hydrogen band EMIC waves, which is different from previous studies [*Meredith et al.*, 2014]. In their research, helium band EMIC waves are observed more frequently than hydrogen band EMIC waves. The reason that leads to this difference is to be found. Figure 6 shows the occurrence rate distribution of helium band EMIC waves in all MLT and from $L = 3$ to $L = 6$. It can be seen that the occurrence rates of helium band EMIC waves have three significant peaks. One peak lies in the noon sector at the $L = 6$, and two peaks occur in the dusk sector. For the two peaks in the dusk sector, one is located at the $L = 3.5$ and 17:00 MLT, which is in an extraordinary low L shell region for the afternoon cases, and the other at

the $L = 4.5–5.5$ and 16:00 MLT. The occurrence rate of helium band EMIC waves in the dawn and night sectors is relatively lower, which is consistent with the statistical results of CRRES observations [*Meredith et al*., 2014].

5. Discussion and Conclusion

Maybe due to the orbit of the satellite, the observation time is limited beyond $L = 5.5$, and the occurrence rate there falls. If this trend does not result from the limit of the orbit, it should be consistent with the conclusion in *Anderson et al*. [1992a]. In their research, there exists a radial separation region at $L = 6$ for the EMIC waves, especially in the morning sector. This characteristic is different from that in *Usanova et al*. [2012]. In their Figure 4, the occurrence rate generally increases with L in the four sectors. This difference may result from the limit of the satellite orbit or the gap for EMIC generation at $L = 6$. The occurrence rate in dusk sector is usually high for $L > 3$, especially for $L > 4.5$; this is consistent with the other studies [*Meredith et al*., 2003; *Usanova et al*., 2012]. The large occurrence rate in the dusk sector may result from the trajectory of the hot ions injected from the magnetotail, and the asymmetric distribution of the plasmapause, which always has a bulge, also called plasmaspheric plume in the dusk sector. This implies the important role of cold dense plasmas in the generation of EMIC waves.

The significant peak in the midnight sector for hydrogen band EMIC waves may imply that the injected hot ions interact with the cold dense plasma in the midnight sector, where the flux of helium ions should be not so high, which needs further investigation. The helium band EMIC waves are more concentrated at the dusk sector, which is consistent with previous studies [*Min et al*., 2012; *Keika et al*., 2013].

Peaks of EMIC wave occurrence in the dawn sector locate at lower L, which implies that some hot ions injected from the magnetotail may pass the dawn sector and continue to move to the midnoon sector directly, consistent with some simulation results [*Jordanova et al*., 2008b].

In the generation of EMIC waves, the temperature anisotropy of energetic ions provides the energy source for ion cyclotron instability [*Cornwall*, 1965], while the presence of cold dense plasma can bring down the threshold of generating EMIC waves [*Criswell*, 1969; *Thorne and Horne*, 1997]. The injected hot ions from the magnetotail are usually temperature anisotropy, and the enhancement of solar wind dynamic pressure can enhance the temperature anisotropy of the hot ions. In addition, the plasmapause and the plasmaspheric plume are the preferable regions where EMIC waves are easily to be generated. The distribution characteristics of EMIC waves in this paper are consistent with the above theories.

At first, the effect of cold dense plasma in the generation of EMIC waves is extensively discussed in both theoretical and observational works [*Thorne and Horne*, 1997; *Chen et al*., 2009; *Yuan et al*., 2010, 2012; *Usanova et al*., 2013]. With the same method as that in Figure 2, we identified the relative position between EMIC wave occurrence region and the outer edge of the plasmapause. As a result, we found that except for six events without plasma density data, all the other events are with plasma density data, and 37% of them were identified outside the plasmasphere and 63% of them inside the plasmasphere. Most of the EMIC wave events were located near the plasmapause. The results implied the important role of the cold dense plasma in the generation of EMIC waves.

Second, the occurrence rate of EMIC waves in the noon sector peaks at the highest L shell, which implies that the solar wind dynamic pressure is also important in the generation of EMIC waves, considering that the compression-related EMIC waves often appear at the noon sector. In higher L regions, the solar wind dynamic pressure may become more important in the generation of EMIC waves [*Usanova et al*., 2008, 2010; *McCollough et al*., 2009, 2012]. The enhancement of solar wind dynamic pressure can increase the temperature anisotropy of energetic ions [*McCollough et al*., 2009, 2012], which can act as the source of cyclotron instability. The enhancement of solar wind dynamic pressure leads to the compression of the magnetosphere in the noon sector more directly and most obviously. Additionally, the extension of plasmaspheric plumes to the noon sector in geomagnetic storms may also favor the generation of EMIC waves there [*Jordanova et al*., 2008a].

Last but not the least, in fact, considerable numbers of EMIC waves occurred in the dawn sector, and many of them were located in the regions with $L < 4$. This implies that in the very inner magnetosphere, the ring current and the plasmasphere may distribute nearly uniformly, and the probability of generating EMIC waves is nearly the same in all sectors where $L < 4$. This implies a possibility that, through wave particle

interaction, EMIC waves may lead to the precipitations of the relativistic electrons not only in the dusk sector but also in the dawn sector, which was thought to be mainly caused by chorus waves in the dawn sector. For instance, the EMIC waves shown in Figure 2 occurred in the dawn sector, and utilizing the quasi-linear theory [*Summers et al.*, 2007], we calculated the pitch angle diffusion rates near the equatorial loss cone for high-energy electrons by the EMIC waves shown in Figure 2. The results (not shown) demonstrate that relativistic electrons with energy higher than 900 keV would resonant with the EMIC waves observed. In another word, the dawn sector EMIC waves shown in Figure 2 could resonant with relativistic electrons with energy higher than 900 keV and make them precipitate into the atmosphere in the future. The research about the wave-particle interaction is beyond the scope of this manuscript, which will be further studied.

In future work, we will examine the relationship between EMIC wave occurrence and solar wind dynamic pressure enhancement, geomagnetic storms, and the plasma density gradient, in order to further understand the generation mechanism of EMIC waves. This would be helpful to establish a general model of EMIC waves in the inner magnetosphere.

Acknowledgments

We acknowledge the Van Allen Probes data from the EMFISIS magnetometer instrument obtained from http://emfisis.physics.uiowa.edu/data/index and the EFW instrument obtained from http://www.space.umn.edu/rbspefw-data/. This research is supported by the National Natural Science Foundation of China (grants 41374168, 41174140, 41221003, and 41174147), research Fund for the Doctoral Program of Higher Education of China (grant 20110141110043), the Fundamental Research Funds for the Central Universities of China (grant 2012212020204), and Program for New Century Excellent Talents in University (NCET-13-0446). The work of M. Zhou was supported by the Science Foundation of Jiangxi Province under grant 20142BCB23006.

Michael W. Liemohn thanks Yonghua Liu and another reviewer for their assistance in evaluating this paper.

References

Anderson, B. J., R. E. Erlandson, and L. J. Zanetti (1992a), A statistical study of Pc1–2 magnetic pulsations in the equatorial magnetosphere: 1. Equatorial occurrence distributions, *J. Geophys. Res.*, *97*, 3075–3088, doi:10.1029/91JA02706.

Anderson, B. J., R. E. Erlandson, and L. J. Zanetti (1992b), A statistical study of Pc1–2 magnetic pulsations in the equatorial magnetosphere: 2. Wave properties, *J. Geophys. Res.*, *97*, 3089–3101, doi:10.1029/91JA02697.

Bortnik, J., R. M. Thorne, T. P. O'Brien, J. C. Green, R. J. Strangeway, Y. Y. Shprits, and D. N. Baker (2006), Observation of two distinct, rapid loss mechanisms during the 20 November 2003 radiation belt dropout event, *J. Geophys. Res.*, *111*, A12216, doi:10.1029/2006JA011802.

Bortnik, J., J. W. Cutler, C. Dunson, and T. E. Bleier (2007), An automatic wave detection algorithm applied to Pc1 pulsations, *J. Geophys. Res.*, *112*, A04204, doi:10.1029/2006JA011900.

Chen, L., R. M. Thorne, and R. B. Horne (2009), Simulation of EMIC wave excitation in a model magnetosphere including structured high-density plumes, *J. Geophys. Res.*, *114*, A07221, doi:10.1029/2009JA014204.

Cornwall, J. M. (1965), Cyclotron instabilities and electromagnetic emission in the ultra low frequency and very low frequency ranges, *J. Geophys. Res.*, *70*(1), 61, doi:10.1029/JZ070i001p00061.

Cornwall, J. M., F. V. Coroniti, and R. M. Thorne (1970), Turbulent loss of ring current protons, *J. Geophys. Res.*, *75*(25), 4699–4709, doi:10.1029/JA075i025p04699.

Criswell, D. R. (1969), Pc1 micropulsation activity and magnetospheric amplification of 0.2- to 5.0-Hz hydromagnetic waves, *J. Geophys. Res.*, *74*, 205–224, doi:10.1029/JA074i001p00205.

Fraser, B. J., and T. S. Nguyen (2001), Is the plasmapause a preferred source region of electromagnetic ion cyclotron waves in the magnetosphere?, *J. Atmos. Sol. Terr. Phys.*, *63*, 1225–1247, doi:10.1016/S1364-6826(00)00225-X.

Fraser, B. J., R. S. Grew, S. K. Morley, J. C. Green, H. J. Singer, T. M. Loto'aniu, and M. F. Thomsen (2010), Storm time observations of electromagnetic ion cyclotron waves at geosynchronous orbit: GOES results, *J. Geophys. Res.*, *115*, A05208, doi:10.1029/2009JA014516.

Gary, S. P., M. F. Thomsen, L. Yin, and D. Winske (1995), Electromagnetic proton cyclotron instability: Interactions with magnetospheric protons, *J. Geophys. Res.*, *100*, 21,961–21,972, doi:10.1029/95JA01403.

Hyun, K., K.-H. Kim, E. Lee, H.-J. Kwon, D.-H. Lee, and H. Jin (2014), Loss of geosynchronous relativistic electrons by EMIC wave scattering under quiet geomagnetic conditions, *J. Geophys. Res. Space Physics*, *119*, 8357–8371, doi:10.1002/2014JA020234.

Jordanova, V. K., C. J. Farrugia, R. M. Thorne, G. V. Khazanov, G. D. Reeves, and M. F. Thomsen (2001), Modeling ring current proton precipitation by electromagnetic ion cyclotron waves during the May 14–16, 1997, storm, *J. Geophys. Res.*, *106*(A1), 7–22, doi:10.1029/2000JA002008.

Jordanova, V. K., H. Matsui, P. A. Puhl-Quinn, M. F. Thomsen, K. Mursula, and L. Holappa (2008a), Ring current development during high speed streams, *J. Atmos. Sol. Terr. Phys.*, *71*, 1093, doi:10.1016/j.jastp.2008.09.043.

Jordanova, V. K., J. Albert, and Y. Miyoshi (2008b), Relativistic electron precipitation by EMIC waves from self-consistent global simulations, *J. Geophys. Res.*, *113*, A00A10, doi:10.1029/2008JA013239.

Keika, K., M. Nose, P. Brandt, S. Ohtani, D. G. Mitchell, and E. C. Roelof (2006), Contributions of charge exchange loss to the storm time ring current decay: IMAGE/HENA observations, *J. Geophys. Res.*, *111*, A11S12, doi:10.1029/2006JA011789.

Keika, K., K. Takahashi, A. Y. Ukhorskiy, and Y. Miyoshi (2013), Global characteristics of electromagnetic ion cyclotron waves: Occurrence rate and its storm dependence, *J. Geophys. Res. Space Physics*, *118*, 4135–4150, doi:10.1002/jgra.50385.

Kletzing, C. A., et al. (2013), The Electric and Magnetic Field Instrument Suite and Integrated Science (EMFISIS) on RBSP, *Space Sci. Rev.*, *179*, 127–181, doi:10.1007/s11214-013-9993-6.

Liu, Y. H., B. J. Fraser, and F. W. Menk (2013), EMIC waves observed by Cluster near the plasmapause, *J. Geophys. Res. Space Physics*, *118*, 5603–5615, doi:10.1002/jgra.50486.

Loto'aniu, T. M., B. J. Fraser, and C. L. Waters (2005), Propagation of electromagnetic ion cyclotron wave energy in the magnetosphere, *J. Geophys. Res.*, *110*, A07214, doi:10.1029/2004JA010816.

McCollough, J. P., S. R. Elkington, and D. N. Baker (2009), Modeling EMIC wave growth during the compression event of 29 June 2007, *Geophys. Res. Lett.*, *36*, L18108, doi:10.1029/2009GL039985.

McCollough, J. P., S. R. Elkington, and D. N. Baker (2012), The role of Shabansky orbits in compression-related electromagnetic ion cyclotron wave growth, *J. Geophys. Res.*, *117*, A01208, doi:10.1029/2011JA016948.

Meredith, N. P., R. M. Thorne, R. B. Horne, D. Summers, B. J. Fraser, and R. R. Anderson (2003), Statistical analysis of relativistic electron energies for cyclotron resonance with EMIC waves observed on CRRES, *J. Geophys. Res.*, *108*(A6), 1250, doi:10.1029/2002JA009700.

Meredith, N. P., R. B. Horne, T. Kersten, B. J. Fraser, and R. S. Grew (2014), Global morphology and spectral properties of EMIC waves derived from CRRES observations, *J. Geophys. Res. Space Physics*, *119*, 5328–5342, doi:10.1002/2014JA020064.

Min, K., J. Lee, K. Keika, and W. Li (2012), Global distribution of EMIC waves derived from THEMIS observations, *J. Geophys. Res.*, *117*, A05219, doi:10.1029/2012JA017515.

Moldin, M. B., L. Downward, H. K. Rassoul, H. K. Rassoul, R. Amin, and R. R. Anderson (2002), A new model of the location of the plasmapause: CRRES results, *J. Geophys. Res.*, *107*(A11), 1339, doi:10.1029/2001JA009211.
Sheeley, B. W., M. B. Moldwin, H. K. Rassoul, and R. R. Anderson (2001), An empirical plasmasphere and trough density model: CRRES observations, *J. Geophys. Res.*, *106*, 25,631–25,641, doi:10.1029/2000JA000286.
Shprits, Y. Y., D. Subbotin, and B. Ni (2009), Evolution of electron fluxes in the outer radiation belt computed with the VERB code, *J. Geophys. Res.*, *114*, A11209, doi:10.1029/2008JA013784.
Su, Z., F. Xiao, H. Zheng, and S. Wang (2010), STEERB: A three-dimensional code for storm-time evolution of electron radiation belt, *J. Geophys. Res.*, *115*, A09208, doi:10.1029/2009JA015210.
Su, Z., F. Xiao, H. Zheng, and S. Wang (2011), CRRES observation and STEERB simulation of the 9 October 1990 electron radiation belt dropout event, *Geophys. Res. Lett.*, *38*, L06106, doi:10.1029/2011GL046873.
Su, Z., H. Zhu, F. Xiao, H. Zheng, C. Shen, Y. Wang, and S. Wang (2012), Bounce-averaged advection and diffusion coefficients for monochromatic electromagnetic ion cyclotron wave: Comparison between test-particle and quasi-linear models, *J. Geophys. Res.*, *117*, A09222, doi:10.1029/2012JA017917.
Su, Z., H. Zhu, F. Xiao, H. Zheng, C. Shen, Y. Wang, and S. Wang (2013), Latitudinal dependence of nonlinear interaction between electromagnetic ion cyclotron wave and radiation belt relativistic electrons, *J. Geophys. Res. Space Physics*, *118*, 3188–3202, doi:10.1002/jgra.50289.
Su, Z., H. Zhu, F. Xiao, H. Zheng, M. Zhang, Y. C. M. Liu, C. Shen, Y. Wang, and S. Wang (2014), Latitudinal dependence of nonlinear interaction between electromagnetic ion cyclotron wave and terrestrial ring current ions, *Phys. Plasmas*, *21*, 052310, doi:10.1063/1.4880036.
Summers, D., and R. M. Thorne (2003), Relativistic electron pitch angle scattering by electromagnetic ion cyclotron waves during geomagnetic storms, *J. Geophys. Res.*, *108*(A4), 1143, doi:10.1029/2002JA009489.
Summers, D., B. Ni, and N. P. Meredith (2007), Timescales for radiation belt electron acceleration and loss due to resonant wave-particle interactions: 2. Evaluation for VLF chorus, ELF hiss, and the electromagnetic ion cyclotron waves, *J. Geophys. Res.*, *112*, A04207, doi:10.1029/2006JA011993.
Thorne, R. M. (2010), Radiation belt dynamics: The importance of wave-particle interactions, *Geophys. Res. Lett.*, *37*, L22107, doi:10.1029/2010GL044990.
Thorne, R. M., and R. B. Horne (1997), Modulation of electromagnetic ion cyclotron instability due to interaction with ring current O+ during magnetic storms, *J. Geophys. Res.*, *102*, 14,155–14,163, doi:10.1029/96JA04019.
Usanova, M. E., I. R. Mann, I. J. Rae, Z. C. Kale, V. Angelopoulos, J. W. Bonnell, K.-H. Glassmeier, H. U. Auster, and H. J. Singer (2008), Multipoint observations of magnetospheric compression-related EMIC Pc1 waves by THEMIS and CARISMA, *Geophys. Res. Lett.*, *35*, L17S25, doi:10.1029/2008GL034458.
Usanova, M. E., et al. (2010), Conjugate ground and multisatellite observations of compression-related EMIC Pc1 waves and associated proton precipitation, *J. Geophys. Res.*, *115*, A07208, doi:10.1029/2009JA014935.
Usanova, M. E., I. R. Mann, J. Bortnik, L. Shao, and V. Angelopoulos (2012), THEMIS observations of electromagnetic ion cyclotron wave occurrence: Dependence on *AE*, *SYMH*, and solar wind dynamic pressure, *J. Geophys. Res.*, *117*, A10218, doi:10.1029/2012JA018049.
Usanova, M. E., F. Darrouzet, I. R. Mann, and J. Bortnik (2013), Statistical analysis of EMIC waves in plasmaspheric plumes from Cluster observations, *J. Geophys. Res. Space Physics*, *118*, 4946–4951, doi:10.1002/jgra.50464.
Usanova, M. E., et al. (2014), Effect of EMIC waves on relativistic and ultrarelativistic electron populations: Ground-based and Van Allen Probes observations, *Geophys. Res. Lett.*, *41*, 1375–1381, doi:10.1002/2013GL059024.
Wang, D. D., Z. G. Yuan, X. H. Deng, M. Zhou, S. Huang, M. Li, H. Li, T. Raita, and Y. Pang (2014), Compression-related EMIC waves drive relativistic electron precipitation, *Sci China Tech. Sci.*, *57*, 2418–2425, doi:10.1007/s11431-014-5701-3.
Wang, Z., Z. Yuan, M. Li, H. Li, D. Wang, H. Li, S. Huang, and Z. Qiao (2014), Statistical characteristics of EMIC wave driven relativistic electron precipitation with observations of POES satellites: Revisit, *J. Geophys. Res. Space Physics*, *119*, 5509–5519, doi:10.1002/2014JA020082.
Yu, X., Z. Yuan, D. Wang, H. Li, S. Huang, Z. Wang, Q. Zheng, M. Zhou, C. A. Kletzing, and J. R. Wygant (2015), In situ observations of EMIC waves in O+ band by the Van Allen Probe A, *Geophys. Res. Lett.*, *42*, 1312–1317, doi:10.1002/2015GL063250.
Yuan, Z., X. Deng, X. Lin, Y. Pang, M. Zhou, P. M. E. Décréau, J. G. Trotignon, E. Lucek, H. U. Frey, and J. Wang (2010), The link between EMIC waves in a plasmaspheric plume and a detached sub-auroral proton arc with observations of Cluster and IMAGE satellites, *Geophys. Res. Lett.*, *37*, L07108, doi:10.1029/2010GL042711.
Yuan, Z., Y. Xiong, D. Wang, M. Li, X. Deng, A. G. Yahnin, T. Raita, and J. Wang (2012), Characteristics of precipitating energetic ions/electrons associated with the wave-particle interaction in the plasmaspheric plume, *J. Geophys. Res.*, *117*, A08324, doi:10.1029/2012JA017783.
Yuan, Z., M. Li, Y. Xiong, H. Li, M. Zhou, D. Wang, S. Huang, X. Deng, and J. Wang (2013), Simultaneous observations of precipitating radiation belt electrons and ring current ions associated with the plasmaspheric plume, *J. Geophys. Res. Space Physics*, *118*, 4391–4399, doi:10.1002/jgra.50432.
Yuan, Z., Y. Xiong, S. Huang, X. Deng, Y. Pang, M. Zhou, I. Dandouras, J. G. Trotignon, A. N. Fazakerley, and E. Lucek (2014), Cold electron heating by EMIC waves in the plasmaspheric plume with observations of the Cluster satellite, *Geophys. Res. Lett.*, *41*, 1830–1837, doi:10.1002/2014GL059241.
Zhang, J.-C., et al. (2014), Excitation of EMIC waves detected by the Van Allen Probes on 28 April 2013, *Geophys. Res. Lett.*, *41*, 4101–4108, doi:10.1002/2014GL060621.
Zhou, Q., F. Xiao, C. Yang, Y. He, and L. Tang (2013), Observation and modeling of magnetospheric cold electron heating by electromagnetic ion cyclotron waves, *J. Geophys. Res. Space Physics*, *118*, 6907–6914, doi:10.1002/2013JA019263.
Zhu, H., Z. Su, F. Xiao, H. Zheng, C. Shen, Y. Wang, and S. Wang (2012), Nonlinear interaction between ring current protons and electromagnetic ion cyclotron waves, *J. Geophys. Res.*, *117*, A12217, doi:10.1029/2012JA018088.

Erratum

In the originally published version of this article, a copy of figure 5 was mistakenly labeled as figure 6. Figure 6 has since been corrected, and this version may be considered the authoritative version of record.